Dust coupling parameter of radio-frequency-discharge complex plasma under microgravity conditions

D. I. Zhukhovitskii,[1,2,*] V. N. Naumkin,[1] A. I. Khusnulgatin,[2,1] V. I. Molotkov,[1] and A. M. Lipaev[1]
[1]*Joint Institute of High Temperatures, Russian Academy of Sciences, Izhorskaya 13, Bd. 2, 125412 Moscow, Russia*
[2]*Moscow Institute of Physics and Technology, 9 Institutskiy per., Dolgoprudny, Moscow Region 141701, Russia*
(Received 8 August 2017; published 6 October 2017)

Oscillation of particles in a dust crystal formed in a low-pressure radio-frequency gas discharge under microgravity conditions is studied. Analysis of experimental data obtained in our previous study shows that the oscillations are highly isotropic and nearly homogeneous in the bulk of a dust crystal; oscillations of the neighboring particles are significantly correlated. We demonstrate that the standard deviation of the particle radius vector along with the local particle number density fully define the coupling parameter of the particle subsystem. The latter proves to be of the order of 100, which is two orders of magnitude lower than the coupling parameter estimated for the Brownian diffusion of particles with the gas temperature. This means significant kinetic overheating of particles under stationary conditions. A theoretical interpretation of the large amplitude of oscillation implies the increase of particle charge fluctuations in the dust crystal. The theoretical estimates are based on the ionization equation of state for the complex plasma and the equation for the plasma perturbation evolution. They are shown to match the results of experimental data processing. Estimated order of magnitude of the coupling parameter accounts for the existence of the solid-liquid phase transition observed for similar systems in experiments.

DOI: 10.1103/PhysRevE.96.043204

I. INTRODUCTION

The ionized gas including dust particles typically in the range from tens of nanometers to thousands of micrometers is commonly called the complex (or dusty) plasmas [1–6]. Such a system makes it possible to study fundamental processes in the strong coupling regime on the kinetic level through the observation of individual particles. In ground-based experiments, gravity has a dominant effect on the structures formed in complex plasmas so that three-dimensional (3D) dust clouds with an adoptable level of the cloud homogeneity cannot be created. In contrast, relatively homogeneous dust particle structures are realized under microgravity conditions either in parabolic flights [7–11] or onboard the International Space Station (ISS) [7,12–17]. Due to the high mobility of electrons, particles acquire a significant (macroscopic) negative electric charge, which leads to the great Coulomb coupling parameter of the dust subsystem Γ [1–6,18,19]. Thus, such a subsystem forms a 3D dust crystal, which, in principle, can undergo phase transitions, in particular, the solid-liquid first-order transition. In the ground-based experiment, such a transition was first observed in study [20].

Although complex plasmas are open nonequilibrium systems, there are grounds to consider a first-order transition observed in the dust subsystem similar to that in an equilibrium system. A close analog of the dust subsystem is a model system known as the one-component plasma (OCP) [21]. Then, one can expect the coupling parameter of the order of 10^2 for the solid-liquid binodal of the dust subsystem. However, under the conditions of PK-3 Plus laboratory onboard the ISS [15,22,23], this parameter amounts to 10^4 due to a significant particle charge. Taking into account the Debye screening of the particle charge cannot reduce this parameter significantly because the Debye length is on the same order as the interparticle distance. Inclusion of the ion-neutral collisions into calculation of the particle charge can reduce Γ at most by an order of magnitude, which is insufficient to account for the solid-liquid binodal (and is incompatible with the particle oscillation amplitude).

We suggest that the particle kinetic temperature that appears in Γ is highly increased as compared to the gas temperature and the temperature of the particle material. Thus, we suggest the anomalous kinetic heating of particles in the dust cloud that takes place under stationary conditions and does not imply the development of instability. Note that the anomalous heating was observed in the two-dimensional (2D) dust crystal [24] and at the bottom of the dust cloud trapped in a striation [25]. In both cases, the overheating was a result of the development of instability. There is evidence that the kinetic temperature of particles in PK-4 experiments is of the order of 0.8 eV [26], which is much higher than the gas temperature but it is still insufficient to reduce Γ properly.

In this study, we continue to analyze the results obtained in the PK-3 Plus experiments [23] and propose the method of determination of the particle kinetic temperature. Based on the Wigner-Seitz cell model for the dust crystal, we show that Γ can be only expressed in terms of the cell radius and the particle radius-vector standard deviation. Thus, the information on the particle charge, which cannot be defined for a dust cloud, and on the particle velocity, which also cannot be determined due to a coarse time resolution of video recording, is unnecessary. We arrive at very high kinetic temperature of the particles in a stationary dust crystal, which proves to be two orders of magnitude higher than that of the gas. We proposed the interpretation of the effect of anomalous heating based on treatment of the particle charge fluctuations that increase significantly the particle oscillation amplitude. On the basis of the ionization equation of state (IEOS) [23,27], which is valid both for the stationary and perturbed local plasma parameters, and of the equation for propagation of a perturbation in the

*dmr@ihed.ras.ru

dust crystal, we show that the charge fluctuations in the dust crystal have much greater amplitude than that for a solitary particle in an infinite plasma. Eventually, we obtain the estimation $\Gamma \sim 10^2$ and demonstrate that this order of magnitude is compatible with the possibility of observation of the solid-liquid phase transition.

The paper is organized as follows. In Sec. II, we propose the method of experimental data processing and analyze the accuracy of particle coordinate determination. In Sec. III, we discuss main peculiarities of the particle oscillation. In Sec. IV, the theory of dust charge fluctuations is developed and the relation between charge fluctuations and the particle oscillation amplitude is revealed. The results of theoretical estimations and of experimental data processing are compared and discussed in Sec. V. The results of this study are summarized in Sec. VI.

II. METHOD OF DETERMINATION OF THE COUPLING PARAMETER FOR THE DUST SUBSYSTEM

Consider a dust cloud in the low-pressure gas discharge under microgravity conditions. We will assume that the coupling parameter for the dust subsystem,

$$\Gamma = \frac{Z_0^2 e^2}{r_d T_d} \gg 1, \tag{1}$$

where Z_0 is the average stationary dust particle charge in units of the electron charge, e is the elementary electric charge, $r_d = (3/4\pi n_d)^{1/3}$ is the Wigner-Seitz radius for the dust particles, n_d is the particle number density, T_d is the dust particle kinetic temperature, and the Boltzmann constant is set to unity. Then the system is indeed a dust crystal, for which the Wigner-Seitz cell model is valid. Within the framework of this model, a particle with finite T_d oscillates in the spherical harmonic potential of its cell. The characteristic oscillation frequency is given by the expression $\omega_0^2 = Z_0^2 e^2/M r_d^3$ [28], where $M = (4\pi/3)\rho_0 a^3$ is the particle mass, ρ_0 and a are the density of particle material and the particle radius, respectively (spherical particles are assumed). For typical experiments with the particles of the diameter $2a = 2.55$ μm (see Sec. III), we have $\omega_0 \simeq 600$ s^{-1}, which exceeds significantly the frequency of video exposure (50 frames/s) for the high-resolution camera used in the PK-3 Plus setup [23]. This means that the particle displacement observed in successive frames must be on the same order as its fluctuation amplitude and, therefore, it is not small enough to determine T_d directly from the particle velocity. Moreover, a direct determination of Z_0 for the dust crystal is also problematic with the available diagnostic tools. However, we will show that the coupling parameter Γ is fully determined by the local number density of particles and their standard deviation from their equilibrium positions δr. Provided that the Wigner-Seitz cell model is valid, these positions coincide with the centers of corresponding cells.

In what follows, we will treat a single particle in the Wigner-Seitz cell with the origin of the coordinate system in its center. If we denote the distance of a particle from the center by r, and its velocity by v, then the average particle potential energy $M\omega_0^2\langle r^2\rangle/2$ is equal to its average kinetic energy $M\langle v^2\rangle/2$. Here, angular brackets denote time averaging. According to the equipartition theorem $M\langle v^2\rangle/2 = 3T_d/2$, which yields $T_d = (Z_0^2 e^2/3r_d^3)\langle r^2\rangle$. We substitute the latter expression in the definition of the coupling parameter to derive

$$\Gamma = \frac{3r_d^2}{\langle r^2\rangle} = 3\left(\frac{r_d}{\delta r}\right)^2, \tag{2}$$

where $\delta r = \sqrt{\langle r^2\rangle}$. It is worth mentioning that Z_0 cancels in the expression (2), therefore, Γ proves to be independent of the particle charge.

We have to keep in mind that δr is a three-dimensional standard deviation while a sequence of video frames provides the information on the projection of the deviation on the frame plane. Note that the method of 3D particle coordinate determination developed in Ref. [23] is not efficient for the particle oscillation because the scan time is orders of magnitude longer than the particle oscillation period $\propto \omega_0^{-1}$. To estimate δr, we assume isotropy of the particle oscillations (which is the case for our system; see Sec. III). Then

$$\delta r = \sqrt{\frac{3}{2}(\langle x^2\rangle + \langle z^2\rangle)}, \tag{3}$$

where x and z are the two-dimensional Cartesian particle coordinates ($\langle x\rangle = \langle z\rangle = 0$ is implied). Hence, (2) can be rewritten in the form,

$$\Gamma = \frac{2r_d^2}{\langle x^2\rangle + \langle z^2\rangle}. \tag{4}$$

Assuming that the dust crystal is stationary, we can estimate $\langle x^2\rangle$ and $\langle z^2\rangle$ from the particle positions observed in successive frames. Obviously, the ratio between the frequency of video exposure and ω_0 does not matter in this case. The Wigner-Seitz radius r_d can be calculated using the method of the local particle number density determination [23].

Below, we will discuss determination of the particle coordinates in individual frames. Since the expected standard deviation is on the same order as the size of a camera pixel ($\sim$10 μm), a satisfactory accuracy of such a procedure is problematic. A favorable circumstance increases the accuracy dramatically. In fact, albeit the particle diameter ($\sim$3 μm) is smaller than a pixel, the light scattered from a particle and passed through the optical system of a video camera form the Gaussian beam with a typical width of 1.5 pixel and, therefore, each particle "illuminates" more than 10 pixels by the light with different intensities. Each pixel codes this light intensity by brightness. If we group together the pixels corresponding to a given particle then we can define the determined particle radius vector as the weighted sum,

$$\mathbf{r} = \frac{\sum_{k=1}^{N} I_k \mathbf{R}_k}{\sum_{k=1}^{N} I_k}, \tag{5}$$

where the sum runs over all pixels pertaining to the selected group, I_k is the brightness of a pixel ($0 \leqslant I_k \leqslant 255$), $\mathbf{R}_k$ is the radius vector of its center. In (5), we have to ignore the pixels with the brightness comparable to the noise brightness ($I_k < I_{\text{th}}$), where $I_{\text{th}} = 20$ for used video camera. It is the information on the pixel brightness involved in (5) that increases the coordinate determination accuracy. We performed a simulation that allows one to estimate this accuracy.

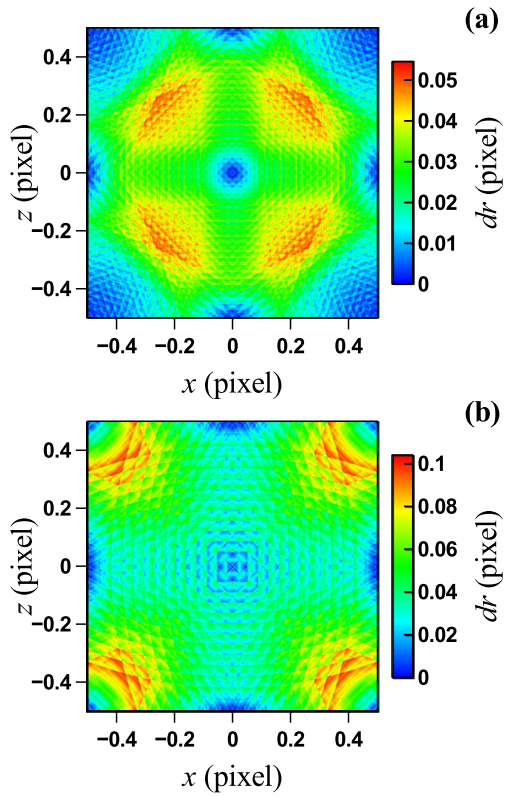

FIG. 1. Distribution of the absolute error involved in the proposed method of particle coordinate determination over the surface area of a pixel. The distance dr between the center of a true Gaussian beam and the determined position of a particle is color coded. The beam amplitude is (a) $A = 100$ and (b) $A = 50$; for both cases, the width is $w = 1.5$ px and the recognition brightness threshold is $I_{\text{th}} = 20$.

A Gaussian beam generates a group of pixels with the brightness distribution,

$$I_k = \left[A \exp\left(-\frac{|\mathbf{R}_k - \mathbf{r}_0|^2}{w^2} \right) \right], \tag{6}$$

for $I_k > I_{\text{th}}$ and $I_k = 0$ otherwise. In Eq. (6), A is the maximum beam intensity, $\mathbf{r}_0$ is the radius vector of the center of a beam that coincides with a true particle radius vector, $w = 1.5$ px is a typical beam width, and square brackets denote an integral part of a number. The distance between the determined and true particle position $dr = |\mathbf{r} - \mathbf{r}_0|$ is shown in Fig. 1 for different $\mathbf{r}_0$ and two characteristic maximum pixel brightnesses. Given $\mathbf{r}_0$, dr was calculated using formulas (5) and (6). This quantity defines the absolute accuracy of the particle coordinate determination. Obviously, showed distribution is periodic in both directions. As is seen, the maximum error dr should be expected if $\mathbf{r}_0$ is varied within a single pixel but even in this case, the relative error is below 10%. This seems to be an appropriate systematic error as compared to the random error, which is noticeably higher (Sec. IV). The error decreases with the increase of A, as it must.

Application of the above-discussed method of the particle coordinate determination allows one to connect the positions of individual particles in a sequence of consecutive frames by lines and thus to obtain a coarse representation of the particle trajectories within their cells (Fig. 2). Here and in what follows, we will assume that the Z axis is directed toward the upper electrode along the symmetry axis of the discharge. The origin of axes XZ is situated in the discharge center. Figure 2(a) shows such trajectories for the entire field of view of the high-resolution camera. In the bottom of this figure, the void boundary is visible and its top corresponds to a boundary between the dust crystal and the electrode sheath, which is beyond the scope of this treatment. If the number of frames for a given particle (particle trace length) is sufficiently large, which corresponds to a long observation time, then the trajectories assume the form of a clew, Fig. 2(b). Analysis of the particle positions makes it possible to investigate the nature of dust particle oscillations.

III. PROPERTIES OF THE DUST PARTICLE OSCILLATIONS

In this section, we will treat a single experiment with the particles of the diameter 2.55 μm at the gas pressure of 10 Pa. The first issue is the time scale of averaging the particle oscillations. Figure 3 shows the standard deviations δx and δz for the coordinates x and z, respectively, averaged over all particles whose trace length exceeds a definite threshold n as a function of this threshold. Here, we assume homogeneity of a dust crystal and perform averaging over all particles in the coordinate range corresponding to Fig. 2. One can see that the slope of both curves changes significantly at $n \approx 40$ frames, which corresponds to 0.8 s, but the deviations determined in the quiescent (laboratory) coordinate system described above are not stationary even after a long time (red curves). This is due to a slow large-scale hydrodynamic motion of the dust crystal caused by vortices [1,29], which shift the centers of the particle's cells. Thus a trend in the positions of particles is formed. Here and in what follows, we will remove this trend by polynomial fitting of the particle coordinates (in most cases, we used cubic polynomials). With trend removal, δx and δz assume stationary values at $n > 40$. As is seen in Figs. 3(a) and 3(b), these values are almost equal, which is indicative of the system isotropy. One can conclude that the data can be statistically significant if the trace length is at least 40 frames. Note that further increase of the threshold trace length decreases the sample size. This conclusion is justified by Fig. 4 that presents 3D deviations of individual particles for different minimum trace lengths. As is seen, beginning with ca. $n = 40$, the scatter of δr becomes moderate and it is almost independent of n. Figure 4 also illustrates the dependence δr on the vertical coordinate. A sharp increase of δr at $z < 3500$ μm is due to the instability that takes place at the void boundary that involves the particles in intense motion. At $z > 6800$ μm, the electrode sheath zone is situated. Here, the dust crystal no longer exists, and characteristic layered structure is visible. Within these limits, δr shows a weak tendency to increase with the increase of z. This means that the dust crystal is, strictly speaking, inhomogeneous with respect to the particle oscillations.

Another illustration of the particle oscillation isotropy and weak inhomogeneity is presented by Fig. 5. In this figure, the deviations δx and δz are shown only for the individual particles with $n > 40$. These data are fitted by the quadratic polynomials. One can see that the fitting curves almost

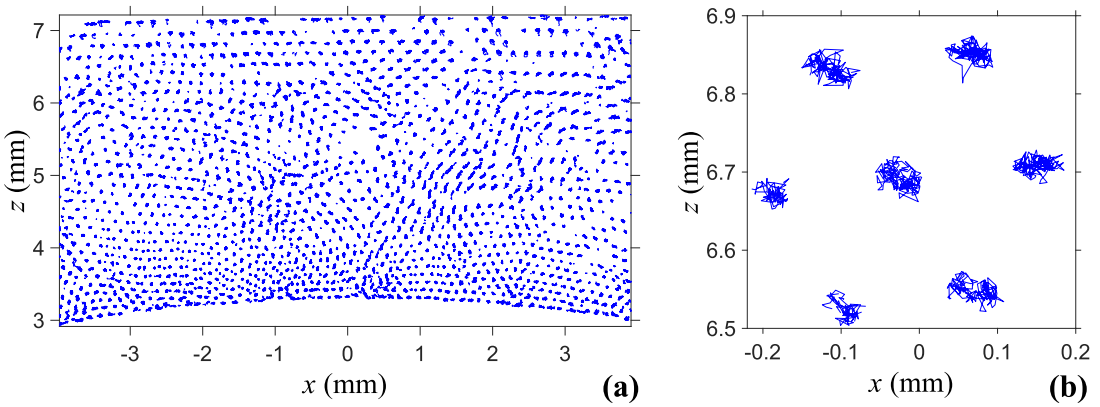

FIG. 2. View of the particle trajectories convoluted into clews obtained by superposition of successive frames. For different trajectories, the trace length varies from 5 to 185 frames. Shown are (a) a view from the high-resolution camera and (b) its enlarged fragment. The origin of the coordinate system coincides with the void center, which finds itself almost at the discharge chamber axis in the middle of the space between the electrodes. The particle diameter is 2.55 μm and the argon pressure is 10 Pa.

coincide, which testifies the system isotropy. More exactly, one can state that within the accuracy of data processing performed in this study, no anisotropy was found. Obviously, the system is homogeneous along the X axis and weakly inhomogeneous along the Z axis.

One more isotropy test is shown in Fig. 6, where the probability distribution over the coordinates is presented. This distribution was calculated from the coordinates of all particles with $n > 40$. It is seen that the distributions over both x and z are almost the same (which provides another evidence of isotropy) and they are well approximated by the Gaussian exponent, whence it follows that the particles indeed oscillate in the 3D harmonic potential. This justifies the use of the Wigner-Seitz cell model. Apparently, slight deviation of the distribution from the Gaussian exponent at its wings arises from the potential anharmonicity at large deviations. It can be the result of some error involved in the trend removal procedure.

Next, consider the correlation of particle oscillations. We failed to estimate the time autocorrelation function for individual particles because the decay time for this function seems to be $\lesssim$0.02 s, i.e., the time interval between successive frames is too long, while calculation of the pair correlation coefficient is possible. We used all pairs of the particles, for which the common part n of the trace lengths is not shorter than 60 frames. Let the positions of a pair of particles be defined by the radius vectors $\mathbf{r}_1 = \{x_1, y_1, z_1\}$ and $\mathbf{r}_2 = \{x_2, y_2, z_2\}$ with the origins in corresponding centers of the Wigner-Seitz cells. The trend is assumed to be removed so that $\langle \mathbf{r}_1 \rangle = \langle \mathbf{r}_2 \rangle = 0$.

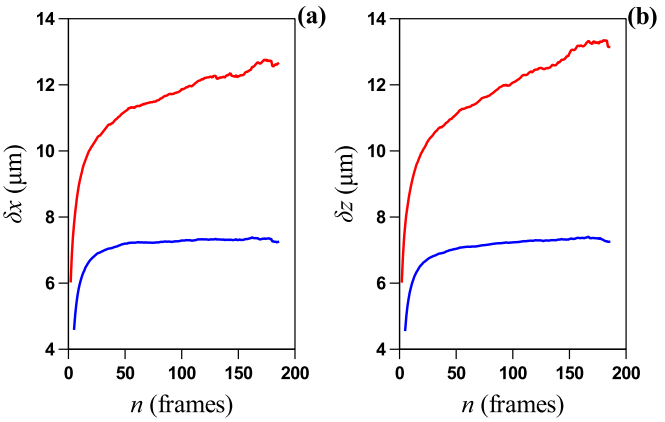

FIG. 3. Standard deviation (a) δx for the coordinate x and (b) δz, for z as a function of the minimum trace length (minimum number of successive frames available for the observation of an individual particle). Lines show the results of averaging over all particle trajectories within the x- and z-coordinate range shown in Fig. 1(a) (field of view of the high-resolution camera); the particle diameter and the gas pressure are the same as in this figure. Blue and red lines indicate the results obtained with and without the trend removal. The particle diameter and the gas pressure are the same as in Fig. 2.

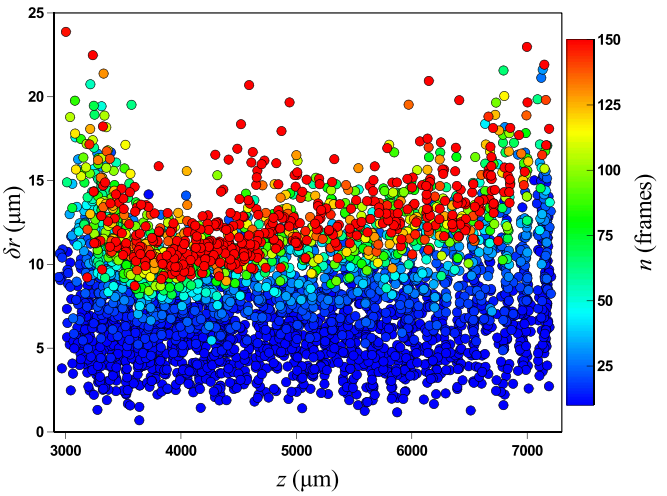

FIG. 4. Three-dimensional standard deviations of particles from its equilibrium positions vs the coordinate z for different minimum trace lengths (color coded). Each point indicates averaging over the trace length of an individual particle. The range of coordinate x corresponds to Fig. 2(a); the particle diameter and the gas pressure are the same as in this figure. For each particle, the trend was removed.

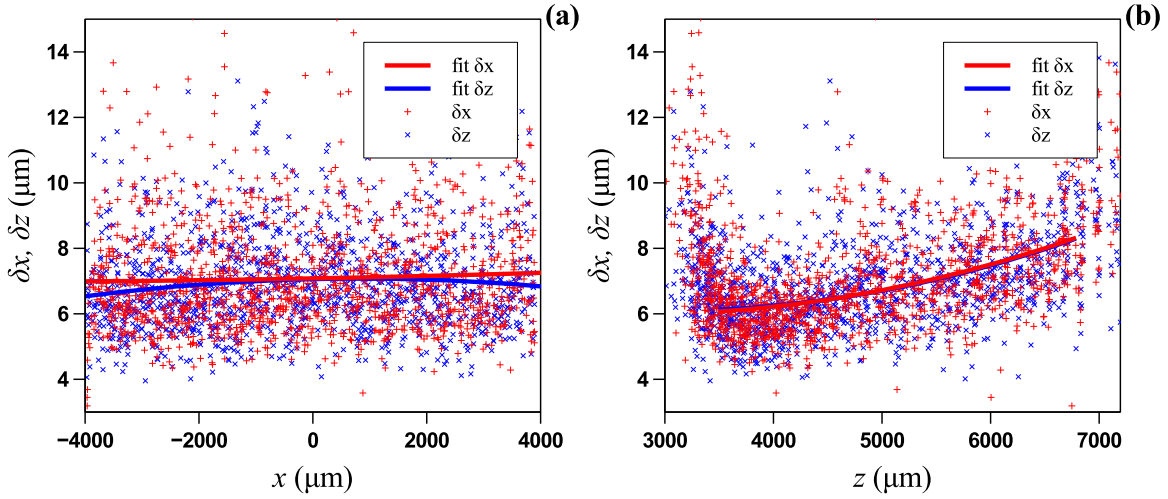

FIG. 5. Standard deviations δx and δz vs (a) the coordinate x and (b) z. Dots show averaging for the individual particles, for which the trace length exceeds 40 frames. The range of particle coordinates z in (a) is the same as the range of the Z axis in (b) and the range of particle coordinates x in (b) is the same as the range of the X axis in (a). Lines show fitting the experimental results by the quadratic polynomials. Red lines and dots indicate δx and blue, δz. The particle diameter and the gas pressure are the same as in Fig. 2.

By definition, the pair correlation coefficient is

$$\kappa = \frac{\sum_{i=1}^{n} \mathbf{r}_{1i} \cdot \mathbf{r}_{2i}}{\sqrt{\sum_{i=1}^{n} r_{1i}^2 \sum_{i=1}^{n} r_{2i}^2}}, \tag{7}$$

where $\mathbf{r}_{1i}$ and $\mathbf{r}_{2i}$ denote the particle radius vectors in the ith frame. In view of a weak inhomogeneity of the system in the z direction (Fig. 5), one can assume the local (small-scale) homogeneity. Due to this and to the global isotropy of the system, we have

$$\frac{1}{n}\sum_{i=1}^{n} x_{1i}x_{2i} \simeq \frac{1}{n}\sum_{i=1}^{n} y_{1i}y_{2i} \simeq \frac{1}{n}\sum_{i=1}^{n} z_{1i}z_{2i}. \tag{8}$$

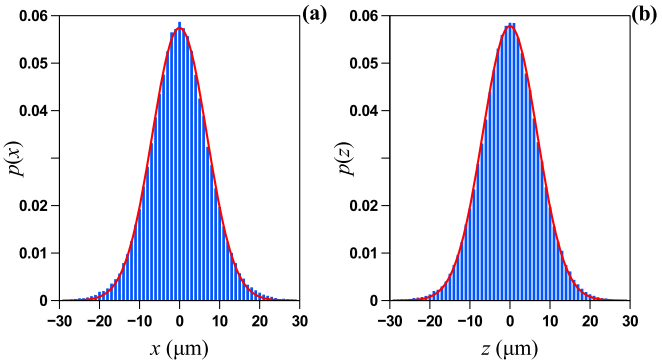

FIG. 6. Probability to find a particle shifted from its equilibrium position (a) in the x direction and (b) in the z direction. Corresponding shifts are Δx and Δz, respectively. The minimum trace length is 40 frames; averaging is performed over all particles in the range shown in Fig. 2(a); the particle diameter and the gas pressure are the same as in this figure.

Since the radius-vector standard deviations δr_1 and δr_2 for the particles 1 and 2 can be expressed as

$$\delta r_{1,2}^2 = \frac{1}{n-1}\left(\sum_{i=1}^{n} x_{1,2i}^2 + \sum_{i=1}^{n} y_{1,2i}^2 + \sum_{i=1}^{n} z_{1,2i}^2\right) \simeq \frac{3}{2}\frac{1}{n-1}\left(\sum_{i=1}^{n} x_{1,2i}^2 + \sum_{i=1}^{n} z_{1,2i}^2\right), \tag{9}$$

we rewrite Eq. (7) in the form,

$$\kappa = \frac{3}{2}\frac{\sum_{i=1}^{n}(x_{1i}x_{2i} + z_{1i}z_{2i})}{(n-1)\delta r_1 \delta r_2}. \tag{10}$$

The pair correlation coefficient averaged over all appropriate pairs of particles is shown in Fig. 7 as a function of the interparticle distance. One can see that at the minimum interparticle distance of 100 μm, the correlation is significant. Apparently, the maxima at $r = 120$ and 250 μm correspond to the first and the second coordination spheres of the dust crystal. If we fit the dependence $\kappa(r)$ by the exponential $\kappa = e^{-r/r_c}$ in the range $100 < r < 450$ μm then we obtain the correlation decay length $r_c = 138$ μm, which is close to the average interparticle distance (under the conditions of treated experiment, it is $n_d^{-1/3} = 145$ μm). At $r > 450$ μm, $\kappa(r)$ decreases to the constant noise level of 0.02 and no correlation peaks are observed. Note that at $r = 450$ μm, $\kappa(r)$ is twice as high as the noise level. It follows from Fig. 7 that the particle oscillation is correlated with that of neighboring particles.

IV. DUST PARTICLE CHARGE FLUCTUATIONS AND THE OSCILLATION AMPLITUDE

As was demonstrated in Sec. III, the particle oscillations are highly isotropic. This means that most likely, they are not related to the ambipolar electric field and the ion flux in complex plasma, neither do they originate from development of an instability. We will assume that the emergence of

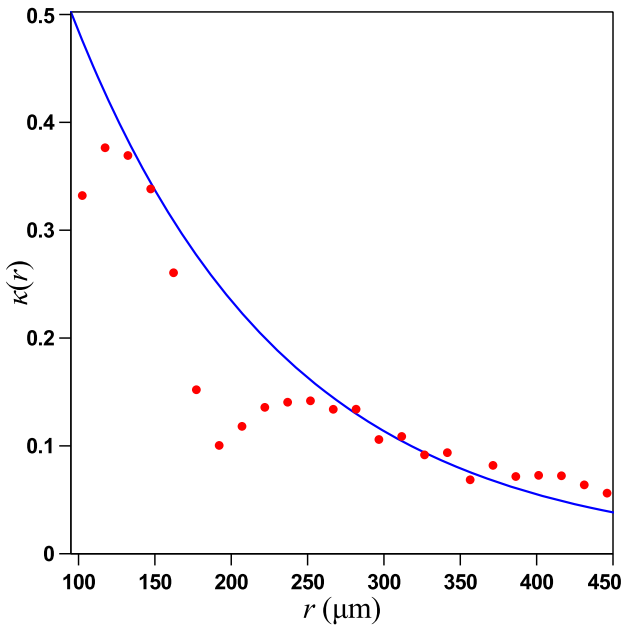

FIG. 7. Correlation coefficient κ vs the interparticle distance r. Dots show averaged experimental results. Averaging was performed over all pairs of particles at the distance within the intervals of 15-μm width. Line indicates the curve fit by exponential. The minimum trace length is 60 frames, the particle coordinate range corresponds to Fig. 2(a), and the particle diameter and the gas pressure are the same as in this figure.

oscillations is caused by the dust particle charge fluctuations and explore the connection between them and the particle oscillations around their equilibrium positions. The system is assumed to conform to the ionization equation of state (IEOS) for complex plasmas with similarity property [23,27,30] based on the fluid approach. The fields of particle velocity $\mathbf{v}(t,\mathbf{r})$ and density $\rho(\mathbf{r}) = Mn_d(\mathbf{r})$ are solutions of the Euler equation,

$$\frac{\partial \mathbf{v}}{\partial t} + (\mathbf{v}\cdot\nabla)\mathbf{v} + \nu\mathbf{v} = \frac{1}{\rho}(\mathbf{f}_e + \mathbf{f}_{id} - \nabla p), \tag{11}$$

and the continuity equation,

$$\frac{\partial \rho}{\partial t} + \nabla\cdot(\rho\mathbf{v}) = 0. \tag{12}$$

Here, $\nu = (8\sqrt{2\pi}/3)\delta m_n n_n v_{T_n} a^2/M$ is the friction coefficient defining the neutral drag [5,31], $\delta \simeq 1.4$ is the accommodation coefficient corresponding to the diffuse scattering of ions against the particle surface, m_n is the mass of a gas molecule, n_n and $v_{T_n} = (T_n/m_n)^{1/2}$ are the number density and the thermal velocity of gas molecules, respectively, $T_n = 300$ K is their temperature,

$$\mathbf{f}_e = -Zen_d\mathbf{E} = -\frac{aT_e}{e}\Phi n_d\mathbf{E} \tag{13}$$

is the electric field driving force acting on unit volume, $\mathbf{E} = (T_e/e)\nabla \ln n_e$ is the electric field strength, T_e is the electron temperature, n_e is the electron number density, and $\Phi = Ze^2/aT_e$ is the dimensionless potential of a dust particle;

$$\mathbf{f}_{id} = \frac{3}{8}\left(\frac{4\pi}{3}\right)^{1/3} n_d^{1/3} n_i \lambda e\mathbf{E} \tag{14}$$

is the ion drag force acting on unit volume, n_i is the ion number density, λ is the ion mean free path with respect to the collisions against gas atoms, and

$$p = \frac{1}{8\pi}\left(\frac{aT_e}{e\lambda^2}\right)^2 p^*, \quad p^* = \Phi^2 n_d^{*4/3} \tag{15}$$

is the dust pressure [30], where $n_d^* = (4\pi/3)\lambda^3 n_d$ is the dimensionless particle number density. For a stationary dust crystal, the force balance equation yields [27,30]

$$\left(\frac{9\pi}{128}\right)^{1/3} \frac{n_i\lambda}{n_d^{2/3}} = \frac{aT_e}{e^2}\Phi. \tag{16}$$

Equation (16) is completed by the equation defining the particle potential that follows from the OML model [32,33],

$$n_e = n_i\theta\Phi e^{\Phi}, \tag{17}$$

where $\theta = \sqrt{T_e m_e/T_i m_i}$, T_i and m_i are the ion temperature and mass, respectively, and m_e is the electron mass.

The equation for small perturbations of a dust crystal can be derived from Eqs. (11) and (12) linearized with respect to small variations of $\mathbf{v}$ and ρ,

$$\frac{\partial^2\psi}{\partial t^2} + \nu\frac{\partial\psi}{\partial t} = c_s^2\Delta\psi, \tag{18}$$

where $\nabla\psi = \mathbf{v}$ and $c_s^2 = dp/d\rho$, where c_s is the velocity of dust acoustic waves (DAWs). As was demonstrated in Ref. [27], c_s is almost independent of the dust density distribution inside the dust crystal and can be treated as a constant,

$$c_s = \frac{aT_e c_s^*}{e\sqrt{6M\lambda}}, \quad c_s^{*2} = \frac{512}{27}\frac{\Phi_s^2(\Phi_s+1)}{(3\Phi_s+4)(\Phi_s+2)}, \tag{19}$$

where Φ_s is the root of the equation,

$$\frac{2\theta e^{\Phi_s}(\Phi_s+1)}{1-\theta\Phi_s e^{\Phi_s}} = 1 + \frac{2}{\Phi_s}. \tag{20}$$

Constancy of the DAWs velocity $dp^*/dn_d^* = c_s^{*2}$ makes it possible to conclude that the relation between the dimensionless ion number density $n_i^* = (e^2\lambda^3/aT_e)n_i$ and n_d^* [23] is

$$\Phi = c_s^*\frac{\sqrt{n_d^* - n_0^*}}{n_d^{*2/3}}. \tag{21}$$

The relation between n_i^* and n_d^* follows from (16) and (21):

$$n_i^* = \frac{2}{\pi}c_s^*\sqrt{n_d^* - n_0^*}. \tag{22}$$

Here, n_0^* is defined by the "dust invariant" κ [23,30],

$$n_0^* = n_f^*\left(1 - \frac{\Phi_f^2 n_f^{*1/3}}{c_s^{*2}}\right), \quad n_f^{*-1} = (a\kappa T_e)^{3/2}\lambda^3. \tag{23}$$

Equations (21) and (22) define the IEOS for a dust crystal. It was demonstrated in [27] that observed isotropy of DAWs in an anisotropic dust crystal has an important consequence. Namely, the variations of all quantities in the perturbation are related by IEOS.

Now turn to the estimation of the charge fluctuations of a dust particle. The equation for particle charge kinetics follows from the balance of the ion and electron fluxes to the particle surface. In the linearized form, this equation reads [1,34]

$$\frac{d\delta Z}{dt} + \nu_f \delta Z = \frac{2Z\nu_f}{1+\Phi_0}\theta(t), \tag{24}$$

where $Z = Z_0 + \delta Z$ is the particle charge, $\langle Z\rangle = Z_0$, and $\langle \delta Z\rangle = 0$ is the charge fluctuation, which is assumed to be small, $|\delta Z/Z_0| \ll 1$, $\nu_f = a v_i(1+\Phi_0)/4r_{Di}^2$ is the charge relaxation frequency, $v_i = \sqrt{8T_i/\pi m_i}$ is the ion thermal velocity, $\Phi_0 = Z_0 e^2/aT_e$, $r_{Di} = \sqrt{T_i/4\pi n_i e^2}$ is the ion Debye length, $\theta(t)$ is a random function that satisfies the conditions,

$$\lim_{t\to\infty}\left[t^{-1}\int_0^t \theta(t)\,dt\right] = 0, \quad \lim_{t\to\infty}\left[t^{-1}\int_0^t \theta^2(t)\,dt\right] = 1. \tag{25}$$

The left-hand side of Eq. (24) is responsible for the charge relaxation while the right-hand side is the source of fluctuations due to discreteness of the ion and electron charges.

Equation (24) is valid for a solitary particle in infinite plasma, where n_i is independent of the charge fluctuations. In contrast, in the dust crystal, the charge fluctuation gives rise to the variation of n_i and n_e at the length scale of the order of r_d around the particle, and it is these quantities that define the particle charging. However, the fluctuation source does not change because it is defined by the averages of n_i and n_e. At the same time, the relaxation frequency ν_f can change dramatically.

In the following, we will derive the equation for the particle charge relaxation neglecting the fluctuation source. If we treat the charge fluctuation as a plasma perturbation then the general equation for its evolution is (18). Although it is based on the fluid approach, it can yield reasonable results even at the length scales of several interparticle distances. Furthermore, we will use this equation for a single cell to derive, at least, an order-of-magnitude estimate for the amplitude of the charge fluctuation. The first term on the left-hand side of (18) corresponds to the perturbation relaxation due to the DAW propagation and the second term, to the diffusive relaxation in the overdamped regime. The corresponding time scales are $\tau_s = r_d/c_s$ and $\tau_{\rm dif} = \nu r_d^2/c_s^2$ [35], respectively. Under the conditions of experiment treated in Sec. III, $\tau_{\rm dif}/\tau_s = \nu r_d/c_s = 0.15$, therefore, the diffusive relaxation dominates. Accordingly, Eq. (18) is reduced to

$$\frac{\partial\psi}{\partial t} = \frac{c_s^2}{\nu}\Delta\psi. \tag{26}$$

Equation (26) has a solution, which decays exponentially in time, $|\mathbf{k}| = r_d^{-1}$, and the function φ satisfies the condition $(c_s^2/\nu)\Delta\varphi = -\varphi/\tau_{\rm dif}$. Then $\chi(t)$ is a solution of the equation,

$$\frac{d\chi}{dt} + \frac{\chi}{\tau_{\rm dif}} = 0. \tag{27}$$

It follows from the relation between the particle pressure perturbation δp and ψ [27] that $\delta p \simeq -M\nu n_d\psi$ in the overdamped regime. Hence, δp also satisfies (27). In view of (15) and (21), $\delta Z \propto \delta\Phi$ follows the same relaxation rule (27): $d\delta Z/dt + \delta Z/\tau_{\rm dif} = 0$. We compare this with the left-hand side of (24) to deduce that for the dust crystal, the relaxation frequency changes from ν_f to $1/\tau_{\rm dif}$. Thus, one can assume that during the time $\tau_{\rm dif}$, the particle motion in the charge space is the Brownian diffusion and the drift motion can be neglected. This diffusion defines the fluctuation amplitude.

Inclusion of the fluctuation source, which is exactly the same as in (24), in the equation for charge evolution, leads to

$$\frac{d\delta Z}{dt} + \frac{\delta Z}{\tau_{\rm dif}} = \frac{2Z_0\nu_f}{1+\Phi_0}\theta(t). \tag{28}$$

Equations (24) and (28) differ only by the relaxation frequency. We apply the fluctuation-dissipation theorem to (28) to derive the standard deviation of charge fluctuations $\sigma_Z Z_0 = \sqrt{\langle \delta Z^2\rangle}$, where

$$\sigma_Z^2 = \frac{\nu_f \nu r_d^2}{(1+\Phi_0)Z_0 c_s^2}. \tag{29}$$

We use (21) and (22) to represent (29) in the form,

$$\sigma_Z^2 = \frac{2a\nu v_i e^2}{\lambda T_i c_s^2}. \tag{30}$$

As is seen from (30), σ_Z is independent of the coordinate. Under typical experimental conditions, it is much higher than that for a solitary particle in infinite plasma $\sigma_Z^{-2} = (1+\Phi_0)Z_0$ [1].

According to the IEOS (21) and (22), the charge fluctuations are related to the standard deviation of the cell radius $\sigma_d r_d = \sqrt{\langle \delta r_d^2\rangle}$. Since it follows from (21) that $\Phi n_d^{*1/6} \simeq c^*$ at $n_d^* \gg n_0^*$, we obtain $\sigma_d = 2\sigma_Z$ with due regard for the relation $\Phi = Ze^2/aT_e$. We recall that according to Fig. 7 the positions of neighboring particles are correlated. If we assume that the change of the cell radius r_d shifts neighboring particles at $\sqrt{\langle \delta r_d^2\rangle}/3$ then we can estimate the standard deviation of the particle radius vector δr as

$$(\delta r)^2 = \frac{8}{9}\frac{a\nu v_i e^2 r_d^2}{\lambda T_i c_s^2}. \tag{31}$$

From (2) and (31), the coupling parameter can be estimated as

$$\Gamma = \frac{27}{8}\frac{\lambda T_i c_s^2}{a\nu v_i e^2}. \tag{32}$$

It follows from (31) and (32) that the relative standard deviation $\delta r/r_d$ and Γ are independent of the coordinate.

V. RESULTS AND DISCUSSION

We used the video frames recorded in experiment Ref. [23] and the particle number density distributions obtained in this study to calculate the radius-vector standard deviation for the dust particles δr and the coupling parameter for the dust subsystem Γ [formulas (3) and (4), respectively] for three sets of the particle radius and argon pressure. The results are summarized in Table I and in Figs. 8–11. As it follows from Table I, δr increases both with the increase in the particle diameter and the gas pressure and these dependencies

TABLE I. Radius-vector standard deviation of the dust particles δr and the coupling parameter of dust subsystem Γ in the center of a dust crystal for the experiments with different particle diameter $2a$, argon pressure p, and the Wigner-Seitz cell radius r_d estimated from experimental data of Ref. [23]. For the relative standard deviation of the particle charge σ_Z and the kinetic dust temperature T_d, theoretical estimations for the conditions of corresponding experiments are presented.

Set No.	$2a$ (μm)	p (Pa)	r_d (μm)	δr (μm)	Γ	σ_Z	T_d (eV)
1	2.55	10	90	12	160	0.144	1.2
2	3.4	11	136	16	220	0.157	3.1
3	3.4	20.5	157	17	250	0.195	4.2

are rather weak. At first sight, the increase of δr with the gas pressure seems to contradict the increase in the friction coefficient ν. However, the behavior of δr is also a result of the change in plasma parameters as the pressure is changed. In particular, the dependencies $n_d(z)$ for different sets are pressure dependent. It is interesting to note that the ratio $\delta r/r_d$ for the sets 1–3 is almost constant and it ranges from 0.13 to 0.11. The plots of δr vs z that were obtained by processing the particle traces ("clews") using formula (3) are shown in Figs. 8–10. In these figures, the regions near the void boundary and the near-electrode sheath are not shown because in the former, the particles are unstable and in the latter, there is no dust crystal. In spite of a significant dispersion of data points, the trend is obvious. In Figs. 8 and 9, δr increases with z and in Fig. 10, δr has a maximum. It can be easily seen that all these dependencies just follow corresponding dependencies $r_d(z)$ (cf. Figs. 5–7, Ref. [23]). The fact that $\delta r/r_d$ is independent of the coordinates follows from Eq. (31). One can see that theoretical estimates agree satisfactory with the results of experimental data processing.

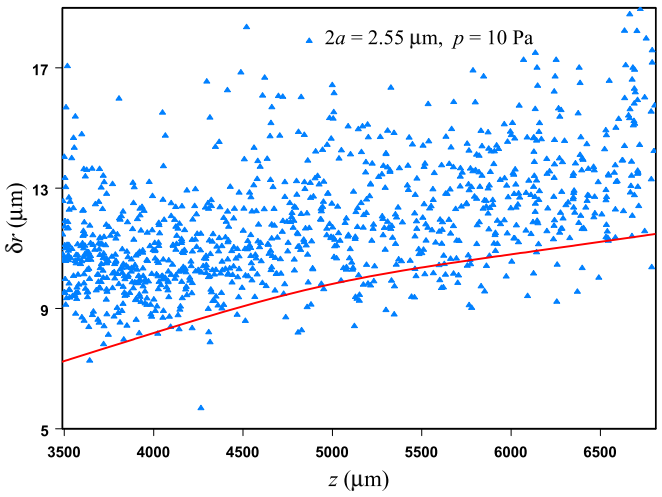

FIG. 8. Three-dimensional standard deviation of a particle from its equilibrium position vs the coordinate z. Dots represent the results of experimental data processing and line shows the calculations using formula (3). The gas pressure, the particle diameter, and the coordinate range are the same as in Fig. 2.

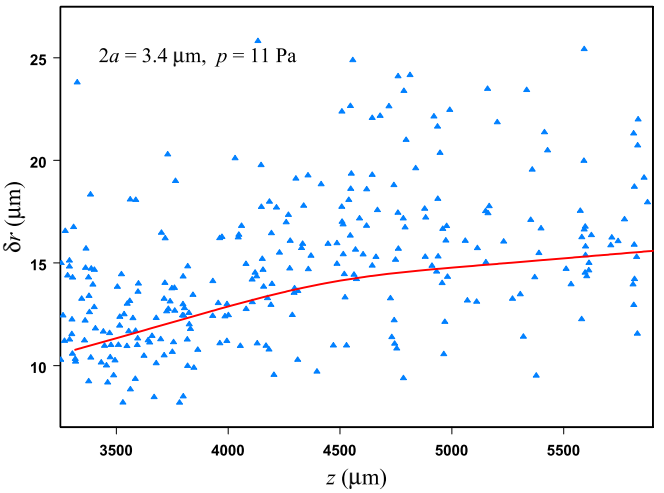

FIG. 9. Same as Fig. 8. The particle diameter is 3.4 μm and the argon pressure is 11 Pa.

For the sets 1–3, the coupling parameter ranges from 160 to 250 (Table I, Fig. 11). This result can be compared with the crystallization threshold for OCP $\Gamma = 168 \pm 4$ [21,36]. Apparently, the dust crystal finds itself far from the solid-liquid binodal, so that for this system, the coupling parameter at binodal must be noticeably lower than for OCP. However, one can testify that $\Gamma \sim 100$ for both systems. This means that the dust crystal is an analog of OCP but these systems are not identical. Note that the same order-of-magnitude estimation ($\Gamma \sim 100$) was reported for the Yukawa ball in the experimental study [37]. Figure 11 illustrates the absence of a noticeable coordinate dependence of the coupling parameter. In Fig. 11, the data points from individual "clews" are averaged within the intervals of z equal to the difference between successive values of the coordinate. The fact that Γ is independent of the coordinate follows from formula (32). One can see that the results of experiment processing lie within the minimum and maximum Γ's (32) calculated for the sets 1–3, i.e., the theory proposed in Sec. IV agrees satisfactorily with

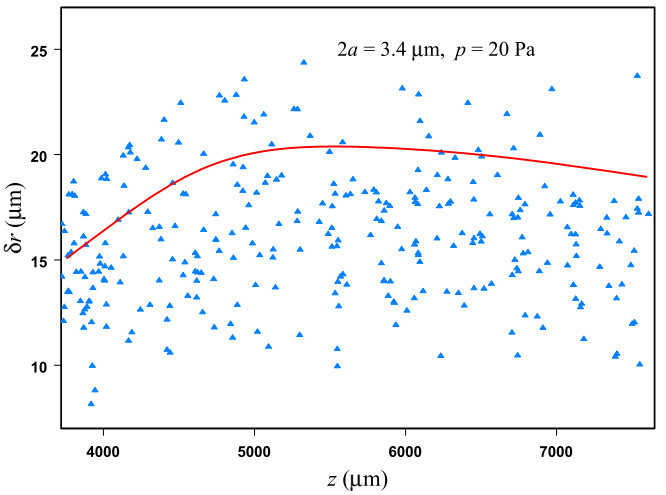

FIG. 10. Same as Fig. 8. The particle diameter is 3.4 μm and the argon pressure is 20.5 Pa.

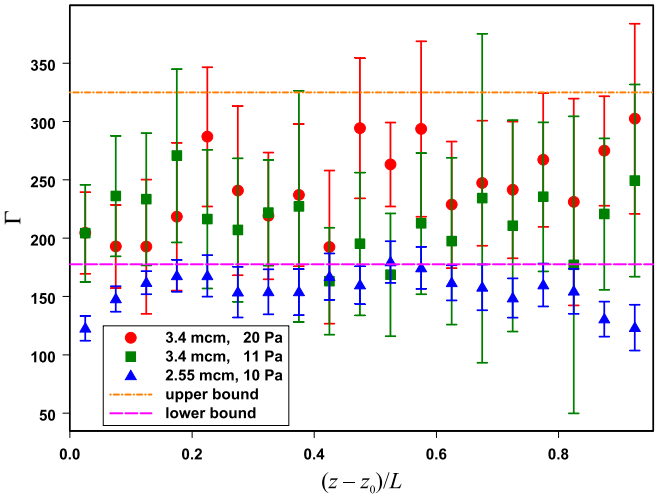

FIG. 11. Coupling parameter for the subsystem of dust particles vs the relative distance from the void boundary along the discharge axis (z_0 is equal to the minimum z for corresponding dust cloud; see Figs. 8–10). Dots represent the results of data processing for different experiments: circles, for $2a = 3.4$ μm and $p = 20.5$ Pa; squares, for $2a = 3.4$ μm and $p = 11$ Pa; and triangles, for $2a = 2.55$ μm and $p = 10$ Pa. Dashed and dash-and-dot line indicate the lower and upper bounds from the theory [formula (4)], respectively, for the above-mentioned experimental conditions.

the experiment. Note that this theory does not match correctly the pressure dependence of Γ. This could be a consequence of (a) simplifying assumptions made, (b) inaccuracy of the IEOS (21) and (22), and (c) a relatively high sensitivity of Γ to p.

Knowledge of Γ allows one to estimate the particle kinetic temperature $T_d = Z_0^2 e^2/r_d\Gamma$ (Table I). Surprisingly, T_d amounts to several eV, which is anomalously high and exceeds the gas temperature T_n by two orders of magnitude. It is noteworthy that the particles in complex plasmas are somewhat overheated due to the ion fluxes to their surface. However, the temperature of particle material cannot exceed ca. 450 K because this is the temperature of evaporation. Some degradation of particles during the experiments was in fact revealed [38]. Thus, high T_d is solely of the kinetic nature, so we can use the term "anomalous kinetic heating." It is important that for the first time, this phenomenon was observed for a stationary 3D dust crystal. In contrast, measurement of the particle velocities in two-dimensional (2D) dust crystals results in the particle kinetic temperature close to room temperature; a substantial increase of this temperature was observed only for the fluid and gaslike states [3,39,40].

The above estimate for the particle kinetic temperature includes the particle charge Z_0, which was estimated using the OML approximation. It was demonstrated that the effect of the ion-neutral collisions [41,42] decreases the calculated particle charge. However, it follows from these studies that this effect is small at the gas pressure less than 30 Pa and $Z_0 n_d/n_e > 1$. Such conditions are typical for the experiments treated in this work. Thus, the particle kinetic temperatures listed in Table I seem to be somewhat overestimated. We recall that the Coulomb coupling parameter Γ (4) needs no correction for this effect because it is independent of Z_0.

The effect of anomalous kinetic heating is a result of relatively high particle charge fluctuations. According to the discussion in Sec. IV the charge fluctuations for a particle in a dust crystal is much larger than that for a solitary particle. As indicated in Table I, the relative standard deviation (30) $\sigma_Z \sim 0.1$ while for a solitary particle it would be an order of magnitude lower, $\sigma_Z = 1/\sqrt{(1+\Phi_0)Z_0} \sim 0.01$.

VI. CONCLUSION

To summarize, we have developed a method of the dust coupling parameter determination that utilizes sequences of video frames recorded in experiments performed on the PK-3 Plus setup. We have demonstrated that the standard deviation of the particle radius vector δr and the particle coupling parameter Γ are defined by solely the standard deviation of the particle radius vectors and the local particle number density. Thus, there is no need for the information on the particle charge and velocity, the oscillation frequency, etc. For the particle number density, we borrowed the distributions determined in our previous study [23]. The peculiarities of analyzed oscillations of particles in their Wigner-Seitz cells are as follows. The oscillations prove to be purely isotropic (within the experimental accuracy) in the entire volume occupied by the dust crystal, which is indicative of the fact that the particle oscillations are not related to the ambipolar electric field and the ion flux in complex plasma. Within the investigated volume, the oscillations are almost homogeneous along the X axis and weakly inhomogeneous in the direction of the Z axis. This mimics exactly the coordinate dependence of the particle number density. The Gaussian form of the probability of particle shift from the center of its cell is indicative of the fact that the particles oscillate in the spherically symmetric quadratic potential. The oscillations of neighboring particles are correlated. Their kinetic temperature is anomalously high and exceeds the gas temperature by two orders of magnitude.

The theoretical interpretation of this anomalous heating implies the effect of particle charge fluctuations. In a dust crystal, the local particle charge and the electron and ion number densities are self-consistent variables. Based on the IEOS and the equation for the perturbation evolution in complex plasma, we have demonstrated that in this case, the amplitude of charge fluctuations is much greater than for a solitary particle in infinite plasma even in the absence of an instability. This amplitude is sufficiently high to ensure a significant effect on the particle oscillation amplitude. Proposed interpretation is rather qualitative because it utilizes a number of crude assumptions like the applicability of the fluid approach at the length scale of the interparticle distance. However, the derived formulas allow one to make order-of-magnitude estimates for the particle standard deviations. Apparently, a more rigorous theory would require the treatment of a self-generated phonon background in the dust crystal. Development of such theory will be addressed in the future.

The theoretical estimates agree satisfactorily with the results of processing the data of experiment [23] and point to the anomalous kinetic heating of particles under stationary conditions. Both the theory and the experiment lead to the particle coupling parameter $\Gamma \sim 100$, which is of the same order as that for OCP at the binodal of the solid-liquid phase

transition. This allows us to account qualitatively for the observed kinetics of phase transition in complex plasma. This investigation can be a basis for the development of a theory of phase transitions in strongly coupled complex plasmas.

ACKNOWLEDGMENT

This research is supported by the Russian Science Foundation, Grant No. 14-12-01235.

[1] V. E. Fortov and G. E. Morfill (eds.), *Complex and Dusty Plasmas: From Laboratory to Space*, Series in Plasma Physics (CRC, Boca Raton, FL, 2010).
[2] J. H. Chu and Lin I, Phys. Rev. Lett. **72**, 4009 (1994).
[3] H. Thomas, G. E. Morfill, V. Demmel, J. Goree, B. Feuerbacher, and D. Möhlmann, Phys. Rev. Lett. **73**, 652 (1994).
[4] S. V. Vladimirov, K. Ostrikov, and A. A. Samarian, *Physics and Applications of Complex Plasmas* (Imperial College, London, 2005).
[5] V. Fortov, A. Ivlev, S. Khrapak, A. Khrapak, and G. Morfill, Phys. Rep. **421**, 1 (2005).
[6] M. Bonitz, C. Henning, and D. Block, Rep. Prog. Phys. **73**, 066501 (2010).
[7] G. E. Morfill, U. Konopka, M. Kretschmer, M. Rubin-Zuzic, H. M. Thomas, S. K. Zhdanov, and V. Tsytovich, New J. Phys. **8**, 7 (2006).
[8] D. Caliebe, O. Arp, and A. Piel, Phys. Plasmas **18**, 073702 (2011).
[9] A. Piel, O. Arp, M. Klindworth, and A. Melzer, Phys. Rev. E **77**, 026407 (2008).
[10] K. O. Menzel, O. Arp, and A. Piel, Phys. Rev. E **83**, 016402 (2011).
[11] O. Arp, D. Caliebe, and A. Piel, Phys. Rev. E **83**, 066404 (2011).
[12] M. Schwabe, S. K. Zhdanov, H. M. Thomas, A. V. Ivlev, M. Rubin-Zuzic, G. E. Morfill, V. I. Molotkov, A. M. Lipaev, V. E. Fortov, and T. Reiter, New J. Phys. **10**, 033037 (2008).
[13] G. E. Morfill, H. M. Thomas, U. Konopka, H. Rothermel, M. Zuzic, A. Ivlev, and J. Goree, Phys. Rev. Lett. **83**, 1598 (1999).
[14] S. A. Khrapak, B. A. Klumov, P. Huber, V. I. Molotkov, A. M. Lipaev, V. N. Naumkin, H. M. Thomas, A. V. Ivlev, G. E. Morfill, O. F. Petrov, V. E. Fortov, Yu. Malentschenko, and S. Volkov, Phys. Rev. Lett. **106**, 205001 (2011).
[15] H. M. Thomas, G. E. Morfill, V. E. Fortov, A. V. Ivlev, V. I. Molotkov, A. M. Lipaev, T. Hagl, H. Rothermel, S. A. Khrapak, R. K. Suetterlin, M. Rubin-Zuzic, O. F. Petrov, V. I. Tokarev, and S. K. Krikalev, New J. Phys. **10**, 033036 (2008).
[16] K. Jiang, V. Nosenko, Y. F. Li, M. Schwabe, U. Konopka, A. V. Ivlev, V. E. Fortov, V. I. Molotkov, A. M. Lipaev, O. F. Petrov, M. V. Turin, H. M. Thomas, and G. E. Morfill, Europhys. Lett. **85**, 45002 (2009).
[17] M. Schwabe, K. Jiang, S. Zhdanov, T. Hagl, P. Huber, A. V. Ivlev, A. M. Lipaev, V. I. Molotkov, V. N. Naumkin, K. R. Sütterlin, H. M. Thomas, V. E. Fortov, G. E. Morfill, A. Skvortsov, and S. Volkov, Europhys. Lett. **96**, 55001 (2011).
[18] Y. Hayashi and S. Tashibana, Jpn. J. Appl. Phys. **33**, L804 (1994).
[19] P. K. Shukla and B. Eliasson, Rev. Mod. Phys. **81**, 25 (2009).
[20] M. Rubin-Zuzic, G. E. Morfill, A. V. Ivlev, R. Pompl, B. A. Klumov, W. Bunk, H. M. Thomas, H. Rothermel, O. Havnes, and A. Fouquét, Nat. Phys. **2**, 181 (2006).
[21] W. L. Slattery, G. D. Doolen, and H. E. DeWitt, Phys. Rev. A **21**, 2087 (1980).
[22] A. G. Khrapak, V. I. Molotkov, A. M. Lipaev, D. I. Zhukhovitskii, V. N. Naumkin, V. E. Fortov, O. F. Petrov, H. M. Thomas, S. A. Khrapak, P. Huber, A. Ivlev, and G. Morfill, Contrib. Plasma Phys. **56**, 253 (2016).
[23] V. N. Naumkin, D. I. Zhukhovitskii, V. I. Molotkov, A. M. Lipaev, V. E. Fortov, H. M. Thomas, P. Huber, and G. E. Morfill, Phys. Rev. E **94**, 033204 (2016).
[24] O. S. Vaulina, S. A. Khrapak, A. P. Nefedov, and O. F. Petrov, Phys. Rev. E **60**, 5959 (1999).
[25] V. V. Zhakhovskii, V. I. Molotkov, A. P. Nefedov, V. M. Torchinskii, A. G. Khrapak, and V. E. Fortov, JETP Lett. **66**, 419 (1997).
[26] A. Usachev, A. Zobnin, O. Petrov, V. Fortov, M. H. Thoma, H. Höfner, M. Fink, A. Ivlev, and G. Morfill, New J. Phys. **16**, 053028 (2014).
[27] D. I. Zhukhovitskii, Phys. Rev. E **92**, 023108 (2015).
[28] D. I. Zhukhovitskii and I. T. Yakubov, Teplofiz. Vys. Temp. (High Temperature) **23**, 842 (1985).
[29] M. Choudhary, S. Mukherjee, and P. Bandyopadhyay, Phys. Plasmas **24**, 033703 (2017).
[30] D. I. Zhukhovitskii, V. I. Molotkov, and V. E. Fortov, Phys. Plasmas **21**, 063701 (2014).
[31] P. Epstein, Phys. Rev. **23**, 710 (1924).
[32] H. M. Mott-Smith and I. Langmuir, Phys. Rev. **28**, 727 (1926).
[33] J. E. Allen, Phys. Scr. **45**, 497 (1992).
[34] V. E. Fortov, A. G. Khrapak, S. A. Khrapak, V. I. Molotkov, and O. F. Petrov, Phys. Usp. **47**, 447 (2004).
[35] D. I. Zhukhovitskii, Phys. Plasmas **24**, 033709 (2017).
[36] S. Hamaguchi, R. T. Farouki, and D. H. E. Dubin, Phys. Rev. E **56**, 4671 (1997).
[37] Y. Ivanov and A. Melzer, Phys. Rev. E **79**, 036402 (2009).
[38] V. Y. Karasev, E. S. Dzlieva, A. P. Gorbenko, I. C. Mashek, V. A. Polishchuk, and I. I. Mironova, Tech. Phys. **62**, 496 (2017).
[39] H. M. Thomas and G. E. Morfill, Nature (London) **379**, 806 (1996).
[40] A. Melzer, A. Homann, and A. Piel, Phys. Rev. E **53**, 2757 (1996).
[41] A. V. Zobnin, A. P. Nefedov, V. A. Sinel'shchikov, and V. E. Fortov, J. Exp. Theor. Phys. **91**, 483 (2000).
[42] S. A. Khrapak, S. V. Ratynskaia, A. V. Zobnin, A. D. Usachev, V. V. Yaroshenko, M. H. Thoma, M. Kretschmer, H. Höfner, G. E. Morfill, O. F. Petrov, and V. E. Fortov, Phys. Rev. E **72**, 016406 (2005).